PROCEEDINGS OF SCIENCE

Average features of the interplanetary shock observed with the Global Muon Detector Network

M. Kozai[a*], K. Munakata[a], C. Kato[a], T. Kuwabara[b], M. Rockenbach[c], A. Dal Lago[d], N. J. Schuch[c], H. K. Al Jassar[e], M. M. Sharma[e], M. L. Duldig[f], J. E. Humble[f], J. W. Bieber[g], P. Evenson[g], I. Sabbah[h] and M. Tokumaru[i]

[a] *Physics Department, Shinshu University, Matsumoto, Nagano 390-8621, Japan.*
[b] *Graduate School of Science, Chiba University, Chiba City, Chiba 263-8522, Japan.*
[c] *Southern Regional Space Research Center (CRS/INPE), P.O. Box 5021, 97110-970, Santa Maria, RS, Brazil.*
[d] *National Institute for Space Research (INPE), 12227-010 São José dos Campos, SP, Brazil.*
[e] *Physics Department, Kuwait University, P.O. Box 5969 Safat, Kuwait 13060.*
[f] *School of Physical Sciences, University of Tasmania, Hobart, Tasmania 7001, Australia.*
[g] *Bartol Research Institute and Department of Physics and Astronomy, University of Delaware, Newark, DE 19716, USA.*
[h] *Department of Natural Sciences, College of Health Sciences, Public Authority of Applied Education and Training, Kuwait City 72853, Kuwait.*
[i] *Solar Terrestrial Environment Laboratory, Nagoya University, Nagoya, Aichi 464-8601, Japan.*
E-mail: 13st303f@shinshu-u.ac.jp, kmuna00@shinshu-u.ac.jp, ckato@shinshu-u.ac.jp, takao@bartol.udel.edu, marlosrs@gmail.com, filhodesun@yahoo.com.br, njschuch@lacesm.ufsm.br, hala.aljassar@ku.edu.kw, madan.sharma@ku.edu.kw, Marc.Duldig@utas.edu.au, john.humble@utas.edu.au, jwbieber@bartol.udel.edu, evenson@UDel.Edu, sabbahsom@yahoo.com, tokumaru@stelab.nagoya-u.ac.jp,

From three-dimensional spatial density gradient of galactic cosmic rays (GCRs) observed with the Global Muon Detector Network (GMDN), we derive average features of the GCR depleted region behind the IP (interplanetary) shock. We identify 207 IP-shocks that passed the earth based on the geomagnetic storm sudden commencements (SSCs) and extract 50 events that are associated with solar coronal mass ejections (CMEs) in a period between 2006 and 2014. From the first order GCR anisotropy corrected for the solar wind convection and Compton-Getting effect arising from the earth's orbital motion, we deduce the density gradient on an hourly basis for each event. We then derive the average temporal variation of the density gradient by superposing its variations at the SSC onset timing. We confirm that the density gradient components are clearly enhanced after the shock passage, indicating the existence of GCR depleted region behind the shock which causes the Forbush Decrease in the cosmic ray intensity. The enhancement of the radial gradient shows longer duration when the earth has encountered the western flank of the shock, implying an asymmetric shielding effect of the shock on the GCRs. The longitudinal gradient, on the other hand, shows that the GCR density minimum is located around the longitudinal center behind the shock, which can be ascribed to the centered ejecta driving IP-shock.

The 34th International Cosmic Ray Conference,
30 July- 6 August, 2015
The Hague, The Netherlands

*Speaker.

PoS(ICRC2015)059

1. Introduction

Short term decreases in the galactic cosmic ray (GCR) isotropic intensity (or density) following the geomagnetic storm sudden commencements (SSCs) were first observed by Forbush, 1937[7] (Forbush Decreases, FDs). In general, the FD starts with a sudden decrease within 3 hours of the SSC onset (Lockwood, 1960[19]), reaches maximum depression within about a day and recovers to the usual level over several days (recovery phase). Most of the decreases follow geomagnetic SSCs, however, the origin of the FD is not the geomagnetic storm but the interplanetary shock (IP-shock) associated with the solar coronal mass ejection (CME) (Obayashi, 1962[23]), which causes the SSC as well (Wang et al., 2006[30]).

Investigating the relation between the heliographic longitude of eruptions and the aspect of FDs, a number of studies (e.g. Sinno, 1962[28]) suggest the east-west asymmetry (E-W asymmetry) of FDs, where the FDs associated with eruptions on the eastern region of the sun disk have larger magnitude and longer duration than western eruptions. The largest FDs with prominent magnitudes, on the other hand, are observed to be associated with eruptions near the central meridian of the Sun as Yoshida and Akasofu, 1965[31] called the "center-limb effect". Cane, 2000[6] gave a comprehensive interpretation including the E-W asymmetry and center-limb effect applying the magnetic configuration model of Hundhausen, 1972[13] to the FDs.

The IP-shocks associated with solar eruptions are known to be driven by the ejected "driver gas" (Hirshberg et al., 1970[12]), i.e. the interplanetary CME. H. V. Cane indicates that the ejecta is only detected for the shock originating near the central meridian (Cane, 1988[3]) while the accompanying shock has a greater longitudinal expansion (Cane et al., 1994[4]). We can ascribe the center-limb effect to the ejecta centered behind the shock which excludes GCRs from its interior. The E-W asymmetry, on the other hand, is assigned to the global shock effect. The interplanetary magnetic field (IMF) has a spiral configuration in the steady state, known as the Parker spiral (Parker, 1958[25]). The compressed IMF in the sheath of the shock, therefore, results in a larger magnitude at the western flank of the shock, reducing the diffusion coefficient of the pitch angle scattering of GCRs (Jokipii, 1971[14]). The sheath with a small diffusion coefficient shields the anti-radial diffusive flow arising from the radial density gradient of GCRs and leads to the deep and long FD at the western side of the shock.

The analysis of the GCR isotropic intensity performed by most of the previous studies, however, shows its limits where it is difficult to separate the dependence of FDs on the eruption's location from that on the event size, because the scalar density only reflects the information on the observation point and does not allow us to infer the three-dimensional structure of the GCR depleted region behind each IP-shock. The spatial density gradient of GCRs, on the other hand, allows us to infer the three-dimensional structure of each depleted region. The direction of the gradient is expected to be independent of the event size if the geometry of the shock is independent of the size, allowing us to reduce the event size dependence which contaminates the dependence on the eruption's location.

The density gradient can be deduced from the first order harmonics of anisotropic intensity (the first order anisotropy) based on Parker's transport equation (Parker, 1965[26]). However, it has been difficult to analyze the dynamic variation of GCR anisotropy associated with IP-shocks, because the traditional analysis is based on the diurnal variation in the cosmic ray counting rate

observed with a single ground-based detector and provides anisotropy on a daily basis as the best time resolution. Only a global network of detectors can measure the dynamic variation of the three-dimensional anisotropy separately from the temporal variation of the isotropic intensity.

The GMDN (Global Muon Detector Network), which is capable of measuring the three-dimensional anisotropy of $\sim$ 60 GeV GCRs on an hourly basis, was completed with four multi-directional muon detectors at Nagoya (Japan), Hobart (Australia), São Martinho da Serra (Brazil), and Kuwait University (Kuwait) in 2006. A new analysis method deducing the hourly first order anisotropy from the GMDN data was first developed by Kuwabara et al., 2004[17]. The advantage of the new analysis method were revealed by Kozai et al., 2014[16], where the new method provides not only the short-term variation but also the long-term variation of anisotropy more accurately than the traditional method. The anisotropy and density gradient associated with the interplanetary disturbances have been investigated by a number of studies (e.g. Kuwabara et al., 2009[18], Fushishita et al., 2010[9], and Rockenbach et al., 2014[27]) using the GMDN. However, all of them are confined to the analysis of individual event or special phenomena such as the magnetic flux rope or precursory anisotropy. In this paper, we perform a statistical analysis of the density gradient observed with the GMDN and reveal the global structure of the GCR depleted region behind the IP-shock.

2. Data analysis

2.1 Derivation of the anisotropy and density gradient

We analyze the pressure corrected hourly count rate $I_{i,j}(t)$ of muons in the j-th directional channel of the i-th detector in the GMDN at the universal time t. Three components $\left(\xi_x^{\mathrm{GEO}}(t), \xi_y^{\mathrm{GEO}}(t), \xi_z^{\mathrm{GEO}}(t)\right)$ of the first order anisotropy in the geographic (GEO) coordinate system are derived by best-fitting following model function to $I_{i,j}(t)$.

$$\begin{aligned} I_{i,j}^{fit}(t) = I_{i,j}^0(t) &+ \xi_x^{\mathrm{GEO}}(t)(c_{1i,j}^1 \cos\omega t_i - s_{1i,j}^1 \sin\omega t_i) \\ &+ \xi_y^{\mathrm{GEO}}(t)(s_{1i,j}^1 \cos\omega t_i + c_{1i,j}^1 \sin\omega t_i) \\ &+ \xi_z^{\mathrm{GEO}}(t) c_{1i,j}^0 \end{aligned} \tag{2.1}$$

where $I_{i,j}^0(t)$ is a parameter representing the contributions from the isotropic intensity and the atmospheric temperature effect, t_i is the local time in hour at the i-th detector, $c_{1i,j}^1$, $s_{1i,j}^1$ and $c_{1i,j}^0$ are the coupling coefficients and $\omega = \pi/12$. The coupling coefficients are calculated using the response function of atmospheric muon intensity to primary cosmic rays (Nagashima, 1971[22], Murakami et al., 1979[21], Fujimoto et al., 1984[8]). In this calculation, we assume a rigidity independent anisotropy with the upper limit rigidity set at 10^5 GV far above the most responsive rigidity of the muon detectors. We additionally apply an analytical method developed to remove the atmospheric temperature effect from the derived anisotropy (see Appendix A1 of Okazaki et al., 2008[24]).

The anisotropy vector is transformed to the geocentric solar ecliptic (GSE) coordinate system and corrected for the solar wind convection effect and the Compton-Getting anisotropy arising from the earth's 30 km/s orbital motion around the sun. We use the solar wind velocity in the OMNI data (King and Papitashvili, 2005[15]) to estimate the convection effect. The corrected anisotropy

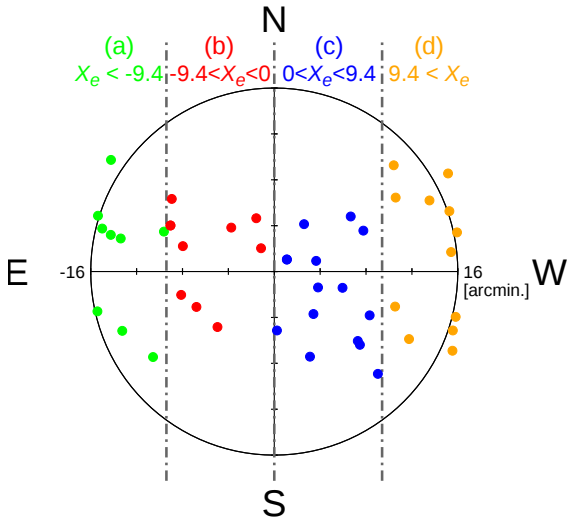

Figure 1: Locations of the solar eruptions associated with analyzed SSCs. Horizontal and vertical axes represent the heliocentric coordinate system on the sky-plane in which left and right sides correspond to east and west sides on the solar surface while top and bottom limbs correspond to north and south poles of the sun. The surrounding circle represents the solar photosphere on the sky-plane with a semi-diameter of 16 arcminute. Solid points divided by vertical lines represent the locations of the solar eruptions in each class, (a) $X_e < -9.4$, (b) $-9.4 < X_e < 0$, (c) $0 < X_e < 9.4$, and (d) $X_e > 9.4$ where X_e arcminute is the horizontal coordinate of an eruption's location.

is expressed using the spatial gradient of the GCR density $U(\boldsymbol{r},t)$ at the earth, $\boldsymbol{G}(t) = \nabla U/U$ as

$$\boldsymbol{\xi}(t) = R_L \left(\alpha_{\parallel} \boldsymbol{G}_{\parallel} + \alpha_{\perp} \boldsymbol{G}_{\perp} - \frac{\boldsymbol{B}}{B} \times \boldsymbol{G}_{\perp} \right) \tag{2.2}$$

where $\boldsymbol{G}_{\parallel}(t)$ and $\boldsymbol{G}_{\perp}(t)$ are the density gradient components parallel and perpendicular to the IMF, $\boldsymbol{B}(t)$ is the IMF vector in the OMNI data, and $R_L(t)$ is the Larmor radius of GCR particles (Gleeson, 1969[10]). $\alpha_{\parallel}$ and $\alpha_{\perp}$ are dimensionless mean free paths ($\lambda_{\parallel}(t)$ and $\lambda_{\perp}(t)$) of the GCR pitch angle scattering, defined as

$$\alpha_{\parallel} = \lambda_{\parallel}(t)/R_L(t) \text{ and } \alpha_{\perp} = \lambda_{\perp}(t)/R_L(t). \tag{2.3}$$

From equation (2.2), the density gradient $\boldsymbol{G}(t)$ is obtained as

$$\boldsymbol{G}(t) = \boldsymbol{G}_{\parallel}(t) + \boldsymbol{G}_{\perp}(t) = \frac{1}{R_L \alpha_{\parallel}} \boldsymbol{\xi}_{\parallel} + \frac{1}{R_L(1+\alpha_{\perp}^2)} \left(\alpha_{\perp} \boldsymbol{\xi}_{\perp} + \frac{\boldsymbol{B}}{B} \times \boldsymbol{\xi}_{\perp} \right) \tag{2.4}$$

where $\boldsymbol{\xi}_{\parallel}(t)$ and $\boldsymbol{\xi}_{\perp}(t)$ are the anisotropy components parallel and perpendicular to the IMF. $R_L(t)$ is calculated as $R_L(t) = R/cB(t)$ where c is light speed and R is the rigidity of GCR particle set at 60 GV. As in Okazaki et al., 2008[24], we assume $\alpha_{\parallel} = 7.2$ and $\alpha_{\perp} = 0.05\alpha_{\parallel}$ based on the numerical solutions by Bieber et al., 1994 and 2004[1, 2].

2.2 Superposed epoch analysis

We deduce average features of the GCR density gradient associated with IP-shocks by superposing its temporal variations obtained from equation (2.4) at the timing of the shock passage.

The IP-shocks are known to cause the geomagnetic SSCs in general (Wang et al., 2006[30]). We identify IP-shock arrivals from the SSCs listed by the German Research Centre for Geosciences (GFZ) and extract 50 CME-associated shocks (CME events) from 207 SSCs in a period between 2006 and 2014, referring to a space weather news (SW news) of the National Institute of Technology, Kagoshima College* (NIT, Kagoshima College) on the date of each SSC occurrence. The SW news has reported current status of the solar surface and interplanetary space each day, monitoring SDO, SOHO, ACE, and GOES satellite data, geomagnetic indices, and solar wind prediction by NOAA/SWPC. It estimates not only the interplanetary origin of each geomagnetic storm but also the associated solar event, allowing us to respectively identify a solar eruption associated with each CME event. After identifying the solar eruptions, we specify their locations on the solar surface referring to the RHESSI flare list as shown in Figure 1. According to the heliocentric horizontal coordinate of each eruption on the sky-plane, X_e arcminute, we classify CME events into (a) $X_e < -9.4$, (b) $-9.4 < X_e < 0$, (c) $0 < X_e < 9.4$, and (d) $X_e > 9.4$. Each class contains (a) 12, (b) 10, (c) 15, and (d) 13 events respectively and we perform a superposed epoch analysis for each class. The heliocentric coordinate border of the classes, 9.4 arcminute is defined to give approximately even event number in each class. The number of eruptions in Figure 1 is a little less than that of SSCs because sometimes one eruption event causes multiple SSCs.

3. Results

Figure 2 shows the superposed temporal variations of the GCR isotropic intensity observed with the neutron monitors (NMs) and the density gradient observed with the GMDN. A gray line shows the temporal variation in each SSC event while black thick and thin lines are the average and standard error deduced from all gray lines at each time. A time interval between the 1st day before the SSC onset and the 3rd day after the onset is covered. The isotropic intensity is deduced by averaging counting rates of two NMs in Thule (Greenland) and McMurdo (Antarctica) as in Suda et al., 1981[29], as

$$U_{\mathrm{NM}} = \frac{U_{\mathrm{Thule}} + U_{\mathrm{McMurdo}}}{2} \tag{3.1}$$

where U_{Thule} and U_{McMurdo} are hourly counting rates of the Thule and McMurdo NMs normalized to the 1 day average before the SSC onset timing. The NM rate U_{NM} indicates the GCR isotropic intensity (i.e. density) approximately free from the anisotropy because the diurnal anisotropy can not have a major effect on the cosmic ray intensity at the polar region and an effect from the north-south anisotropy is canceled by averaging counting rates at the two poles. In Figure 2, NM rate shows a rapid decrease after the SSC onset and then recovers to the usual level over more than 3 days in all classes, i.e. FD. The time profile of FD shows a clear dependence on the location of the solar eruption as found by Sinno, 1962[28] and Cane et al., 1994[4] where the decrease and recovery rate are slower in the eastern eruption event (class (a)) while class (d) shows the most rapid decrease and recovery.

Before the SSC onset, G_x has an offset of $\sim$ -1 %/AU while G_y and G_z are around zero in Figure 2, showing well-known radial density gradient in the steady state arising from the heliocentric solar wind convection of the GCR particles (cf. Munakata et al., 2014[20]). After the SSC onset, G_x

*http://www.kagoshima-ct.ac.jp/

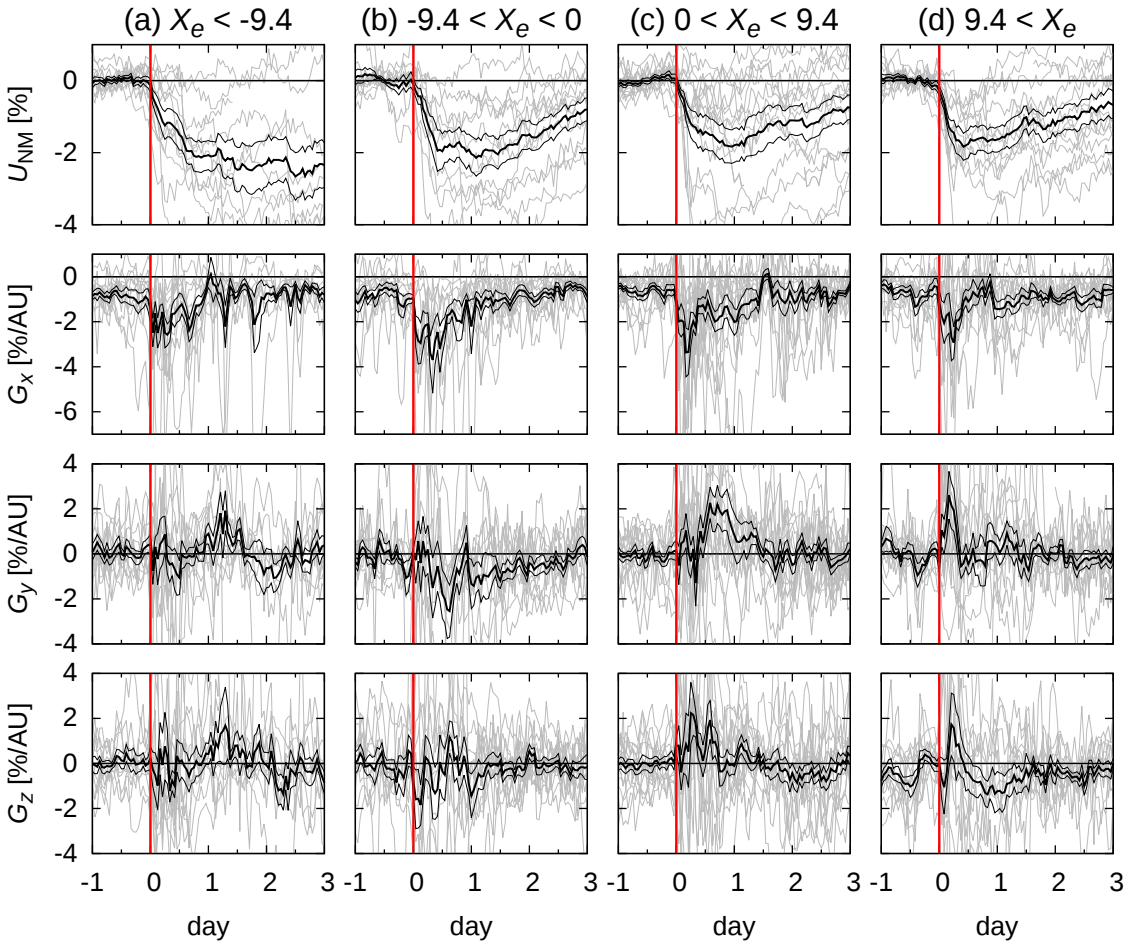

Figure 2: Superposed temporal variations of the cosmic ray parameters in the CME event classified into (a), (b), (c) and (d) classes. Horizontal axes represent the relative time to each SSC onset timing set at 0 day with the vertical red lines, where positive and negative days indicate the time after and before the SSC onset. A gray line shows the temporal variation in each SSC event while black thick and thin lines are the average and standard error deduced from all gray lines at each time. Each panel from top to bottom displays the GCR isotropic intensity observed with the NMs and x, y and z components of the density gradient in the GSE coordinate system observed with the GMDN.

shows a clear negative enhancement, indicating that the earth encounters the GCR depleted region behind the shock propagating antisunward. We can see that its duration time is dependent on the location of the solar eruption where it is longer in classes (a) and (b) than in classes (c) and (d). The GSE-y component (opposite to the earth's orbital motion, i.e. the eastward direction), G_y also shows an enhancement after the SSC onset. G_y is enhanced to the positive direction for ~ 6 hours after the SSC onset only in class (d) and after that, enhanced to negative and positive directions in classes (b) and (c).

The SSC event associated with an eastern (western) solar eruption involves the earth encountering the western (eastern) flank of the shock. The positive (i.e. eastward) G_y enhancement in the western eruption events ((c) and (d)) and the negative (westward) one in the eastern eruption

event (b), therefore, imply that the GCR density minimum is located around the longitudinal center behind the shock, supporting the result of Yoshida and Akasofu, 1965[31], the center-limb effect. On the other hand, slower G_x enhancement in the eastern eruption events and significant but short G_y enhancement in class (d) imply that the GCR depleted region has a large spread in its western side and is narrow and compressed in the eastern side, indicating the E-W asymmetry of the shock effect proposed by Haurwitz et al., 1965[11]. These are partially supported by the east-west dependence of the NM rate mentioned above, however, NM rate shows the most reduced density in the eastern eruption event (class (a)) on average, compared with the center-limb effect.

The north-south component G_z, on the other hand, shows no systematic dependence on the longitudinal location of the solar eruption, while the large dispersion after the SSC onset indicates the existence of G_z enhancement.

4. Summary and discussions

A number of researchers have performed statistical analyses for the FDs, however, most of them analyzed only the isotropic intensity, i.e. the GCR density. In this study, we have analyzed statistically not only the GCR density but also its spatial gradient associated with the IP-shocks for the first time. The GCR density gradient allows us to infer the three-dimensional structure of GCR depleted region behind each IP-shock, while the scalar density has only the information on the observation point. We have derived the density gradient from the first order anisotropy observed with the GMDN which is capable of providing the GCR anisotropy on an hourly basis. 50 CME-associated shocks were identified for analysis in a period between 2006 and 2014 and we have performed a superposed epoch analysis of the density gradient for them.

The radial density gradient is enhanced at the timing of SSC onset in all classes of the eruption's location, indicating that the earth encountered the GCR depleted region which causes FD. The average temporal variation of the density gradient indicates two features of the depleted region behind the shock:

- The depleted region is asymmetric with a larger spread in its western side (E-W asymmetry). This implies an asymmetric shielding effect of the shock on the GCR particles where the compressed plasma in the sheath of the shock has a smaller diffusion coefficient of GCRs in the western flank as proposed by Haurwitz et al., 1965[11].

- The density minimum is located around the longitudinal center behind the shock (center-limb effect) in spite of the asymmetric shock effect. This is interpreted as the solar ejecta (interplanetary CME) centered behind the shock causing the most depleted region as indicated by Cane et al., 1996[5].

The NM rate shows the deepest FD in the eastern eruption events (a) compared with the center-limb effect, however, the dependence of the average depth on the eruption's location seems insignificant with a large dispersion as shown in Figure 2. We can ascribe a major part of this dispersion to the dependence on the event size. The GSE-y component G_y of the density gradient, on the other hand, is significantly enhanced to the opposite directions in the eastern (b) and western (c) events because the vector direction, which indicates the three-dimensional geometry, is not affected by the event size, allowing us to discuss the structure of the depleted region with a greater significance.

Acknowledgments

This work is supported in part by the joint research programs of the Solar-Terrestrial Environment Laboratory (STEL), Nagoya University and the Institute for Cosmic Ray Research (ICRR), University of Tokyo. The observations are supported by Nagoya University with the Nagoya muon detector and CNPq, CAPES, INPE and UFSM with the São Martinho muon detector. The Kuwait muon telescope is supported by the project SP01/09 of the Research Administration of Kuwait University. Neutron monitors of the Bartol Research Institute are supported by the National Science Foundation grant ATM-0000315. The OMNI data were obtained from the GSFC/SPDF OMNIWeb interface at http://omniweb.gsfc.nasa.gov. The SSC list was obtained from Helmholtz-Centre Potsdam - GFZ via the website at http://www.gfz-potsdam.de. RHESSI flare list is provided by NASA/GSFC via the website http://hesperia.gsfc.nasa.gov. The SW news was provided by National Institute of Information and Communications Technology (NICT) until 2009 and is currently provided by NIT, Kagoshima College. We thank M. Shinohara for updating the SW news every day.

References

[1] Bieber, J. W., W. H. Matthaeus, and C. W. Smith, 1994, *Astrophys. J.* **420**, 294-306.

[2] Bieber, J. W., W. H. Matthaeus, and A. Shalchi, 2004, *Geophys. Res. Lett.* **31**, L10805.

[3] Cane, H. V., 1988, *J. Geophys. Res.* **93**, 1-6.

[4] Cane, H. V., I. G. Richardson, and T. T. von Rosenvinge, 1994, *J. Geophys. Res.* **99**, 21,429-21,441.

[5] Cane, H. V., I. G. Richardson, and T. T. von Rosenvinge, 1996, *J. Geophys. Res.* **101**, 21,561-21,572.

[6] Cane, H. V., 2000, *Space Sci. Rev.* **93**, 55-77.

[7] Forbush, S. E., 1937, *Phys. Rev.* **51**, 1108-1109.

[8] Fujimoto, K., A. Inoue, K. Murakami, K. Nagashima, 1984, *Rep. Cosmic-Ray Res. Lab.* **9**.

[9] Fushishita, A. et al., 2010, *Astrophys. J.* **715**, 1239-1247.

[10] Gleeson, L. J., 1969, *Planet. Space Sci.* **17**, 31-47.

[11] Haurwitz, M. W., S. Yoshida, and S.-I. Akasofu, 1965, *J. Geophys. Res.* **70**, 2977-2988.

[12] Hirshberg, J., A. Alksne, D. S. Colburn, S. J. Bame, and A. J. Hundhausen, 1970, *J. Geophys. Res.* **75**, 1-15.

[13] Hundhausen, A. J., 1972, *Solar Wind*, C. P. Sonett et al. (eds.), NASA *Spec. Publ. SP* **308**, 393-417.

[14] Jokipii, J. R., 1971, *Rev. Geophys. Space Phys.* **9**, 27-87.

[15] King, J. H., and N. E. Papitashvili, 2005, *J. Geophys. Res.* **110**, A02104.

[16] Kozai, M. et al., 2014, *Earth, Planets and Space* **66**, 151.

[17] Kuwabara, T. et al., 2004, *Geophys. Res. Lett.* **31**, L19803.

[18] Kuwabara, T. et al., 2009, *J. Geophys. Res.* **114**, A05109.

[19] Lockwood, J. A., 1960, *J. Geophys. Res.* **65**, 3859-3880.

[20] Munakata, K., M. Kozai, C. Kato, and J. Kóta, 2014, *Astrophys. J.* **791**, 22.

[21] Murakami, K., K. Nagashima, S. Sagisaka, Y. Mishima, A. Inoue, 1979, *IL Nuovo Cimento* **2C**, 635-651.

[22] Nagashima, K., 1971, *Rep. Ionos. Space Res. Japan* **25**, 189-211.

[23] Obayashi, T., 1962, *J. Geophys. Res.* **67**, 1717-1729.

[24] Okazaki, Y. et al., 2008, *Astrophys. J.* **681**, 693-707.

[25] Parker, E. N., 1958, *Astrophys. J.* **128**, 664-676.

[26] Parker, E. N., 1965, *Planet. Space Sci.* **13**, 9-49.

[27] Rockenbach, M. et al., 2014, *Space Sci. Rev.* **182**, 1-18.

[28] Sinno, K., 1962, *J. Phys. Soc. Japan* **17** Suppl. A-II, 395-399.

[29] Suda, T., and M. Wada, 1981, *proc. ICRC 1981*, SH 8.2-15.

[30] Wang, C., C. X. Li, Z. H. Huang, and J. D. Richardson, 2006, *Geophys. Res. Lett.* **33**, L14104.

[31] Yoshida, S. and S.-I. Akasofu, 1965, *Planet. Space Sci.* **13**, 435-448.